

# Optical signatures of bulk g-wave altermagnetism in MnTe

Luca Haag,<sup>1</sup> Marius Weber,<sup>2,1</sup> Kai Leckron,<sup>1</sup> Libor  
Šmejkal,<sup>3,4</sup> Jairo Sinova,<sup>2</sup> and Hans Christian Schneider<sup>1</sup>

<sup>1</sup>*Department of Physics and Research Center OPTIMAS,*

*University of Kaiserslautern-Landau, 67663 Kaiserslautern, Germany*

<sup>2</sup>*Institut für Physik, Johannes Gutenberg University Mainz, 55099 Mainz, Germany*

<sup>3</sup>*Max Planck Institute for the Physics of Complex Systems, 01187 Dresden, Germany*

<sup>4</sup>*Max Planck Institute for Chemical Physics of Solids, 01187 Dresden, Germany*

(Dated: May 19, 2025)

# Abstract

In planar altermagnets, optical excitation by linearly polarized ultrashort pulses can induce spin polarizations in the electronic excited states in a controlled fashion, even though the material is magnetically compensated. Here, we theoretically analyze the response of the prototypical bulk  $g$ -wave altermagnet  $\alpha$ -MnTe to polarized ultrashort pulses. By calculating the excited electron distributions based on ab-initio band structure data, we show how this excited electronic spin response in  $\alpha$ -MnTe exhibits different symmetries which are determined by the nodal planes intrinsic to the bulk  $g$ -wave altermagnet. We present a simple procedure to obtain the symmetry of the electronic spin response from the two-dimensional cuts through the three-dimensional band structure.

## I. INTRODUCTION

Altermagnets promise new spin-dependent functionalities due their unique properties favorable for spintronics applications. These include not only the combination of ferromagnetic splitting, antiferromagnetic zero net magnetization and THz dynamics, but also unique spintronics response due to their nodal  $d$ ,  $g$ , or  $i$ -wave spin order [1, 2]. Their spin-split bands in momentum space make it possible to efficiently control electronic spins while their vanishing net magnetic moment protects the spin information against unwanted external disturbances. Extensive research efforts are being made in order to screen the large number of altermagnetic candidate materials, including insulators and semiconductors but also metals, for their use in spintronics [2–5].

At present, the semiconducting compound  $\alpha$ -MnTe [1] is one of the most prominent materials for the study of altermagnetism. While for another popular altermagnetic candidate material RuO<sub>2</sub> there is considerable debate as to which structures show  $d$ -wave altermagnetism [6–9], the altermagnetic character of MnTe has been experimentally confirmed through anomalous Hall effect measurements [10] and anisotropic magneto resistance measurements [11]. Moreover, its nodal bulk  $g$ -wave spin order was directly observed in the spin-dependent band splitting by angle-resolved photo emission spectroscopy (ARPES) by several groups [12–14]. Furthermore, X-ray magnetic circular dichroism has been used to characterize this altermagnet [15], and a series of theoretical and experimental investigations have focused on its transport properties [11, 16, 17].

Apart from its transport properties MnTe also serves as a prototypical altermagnetic

material to study the optical response on ultrafast timescales since the domain size is on the order of several microns [18]. We recently showed using *ab-initio* based calculations for  $\text{RuO}_2$  and  $\text{KRu}_4\text{O}_8$  that non-equilibrium spin densities can be injected by *linearly* polarized laser pulses in planar d-wave altermagnets [19, 20]. This non-equilibrium effect can be detected using magneto-optical techniques even for Néel vector orientations for which static MOKE is forbidden by symmetry [21], as we were able to demonstrate by time-resolved magneto-optical Kerr measurements [19] on  $\text{RuO}_2$  thin films. The possibility to coherently control the induced spin polarization in such a compensated material by the linear polarization state of the exciting laser pulse is a robust effect rooted in the altermagnetic symmetries that has also been obtained in other theoretical studies [22–24]. In addition, phonon and magnon contributions, which are secondary effects following the optical excitation, have been identified on picosecond timescales in magneto-optical Kerr effect measurements depending on the light polarization [25].

These existing results motivate a study of spin dependent optically excited electron dynamics of a prototypical g-wave altermagnet on ultrafast timescales. Due to the additional vertical and horizontal nodal planes in a bulk g-wave altermagnet compared to the planar d-wave variant, one can expect the optically induced effects to be very different in these two altermagnetic systems. Our goal here is, therefore, to theoretically analyze the optical response of the bulk g-wave altermagnet  $\alpha\text{-MnTe}$ . We present a detailed study of the dependence of the spin polarization on polarization angle and wavelength of the exciting ultrashort pump pulses. Our results are also intended to guide potential magneto-optical measurements.

We first discuss the calculated electronic ground-state properties of  $\text{MnTe}$  and its specific altermagnetic symmetries. In the following sections, we then characterize the spin-dependent electronic response of this system.

## II. ELECTRONIC GROUND STATE

In this section, we focus on the electronic band structure and the dipole matrix elements of  $\alpha\text{-MnTe}$ . They were determined *ab initio* by density-functional calculations with the ELK all-electron LAPW code [26] using the PBE generalized gradient approximation (GGA) [27]. Correlation effects were included via the DFT+U approach [28]. Figure 1a depicts

the structure of  $\alpha$ -MnTe, which crystallizes in the hexagonal space group  $P6_3/mmc$  [10, 29], with the lattice constants  $a = 4.134 \text{ \AA}$  and  $c = 6.652 \text{ \AA}$ . We set the Néel vector (pink arrow) orientation along the  $[1\bar{1}0]$ -direction of the crystal, which is one of the easy axis orientations [29]. The magnetic character of the manganese(Mn) atoms is highlighted by red (spin up) and blue (spin down), respectively. Importantly, the nonmagnetic tellurium(Te) atoms (gray) form an octahedral crystal environment that breaks the pure translational symmetry between the two magnetic sublattices.

The spin-group [1, 30] is  $^26/2m^2m^1m$  and the sublattices are connected by the  $[C_2||C_{6z}t_{1/2}]$  operation, which consists of a translation along the  $z$ -axis by half a lattice vector combined with a  $60^\circ$  rotation (screw symmetry) in real space accompanied by an inversion in spin space. These symmetries result in the formation of four spin-degenerate nodal planes in  $k$ -space. Figure 1b shows the Brillouin zone of  $\alpha$ -MnTe that exhibits as the defining feature of the bulk g-wave character three vertical nodal planes and one horizontal nodal plane (gray). The pink lines show the high symmetry path  $L^* - \Gamma - L$  and the corresponding band structure along this path is depicted in Fig. 1c. Overlaid on the band structure is a color code for the spin expectation value,  $\langle s_{\mathbf{k},\mu}^y \rangle$ , of the electronic Bloch state with momentum  $\mathbf{k}$  and band index  $\mu$  projected on the Néel vector direction ( $y$ -direction). Here, dark red indicates an orientation parallel to the  $y$ -axis, while dark blue indicates an antiparallel alignment. We will refer to these as “spin-up” and “spin-down” in the following. The white regions represent spin-mixed regions that arise due to spin-orbit coupling (SOC). The bands along the paths  $L^* - \Gamma$  and  $\Gamma - L$  have the same form as a function of energy but exhibit the typical alternating spin pattern. Figs. 1d and 1e show the spin texture of the uppermost band below the Fermi energy in two-dimensional cross sections of the Brillouin zone where Fig. 1d shows a  $(k_x, k_y)$ -plane with  $k_z \neq 0$ , which is outside the horizontal nodal plane, and Fig. 1e depicts a plane perpendicular to the  $k_x$ -axis that intersects the  $\Gamma$  point. The spin structure of the cross section in Fig. 1d is divided by the three vertical nodal planes into six areas with alternating spin orientation. The regions opposite to each other, i.e., when transforming from  $(k_x, k_y, k_z)$  to  $(-k_x, -k_y, k_z)$ , show a reversed spin character. The spin structure of the  $k_y$ - $k_z$  plane in Fig. 1e is divided into four areas with alternating spin orientation. Interestingly, the spin character for areas opposite in  $k$ -space are now identical. This specific “planar d-wave like” spin pattern is reminiscent of that of planar d-wave altermagnets such as  $\text{RuO}_2$  and  $\text{KRu}_4\text{O}_8$  [1], for which we have demonstrated that the excited spin polarization can be controlled

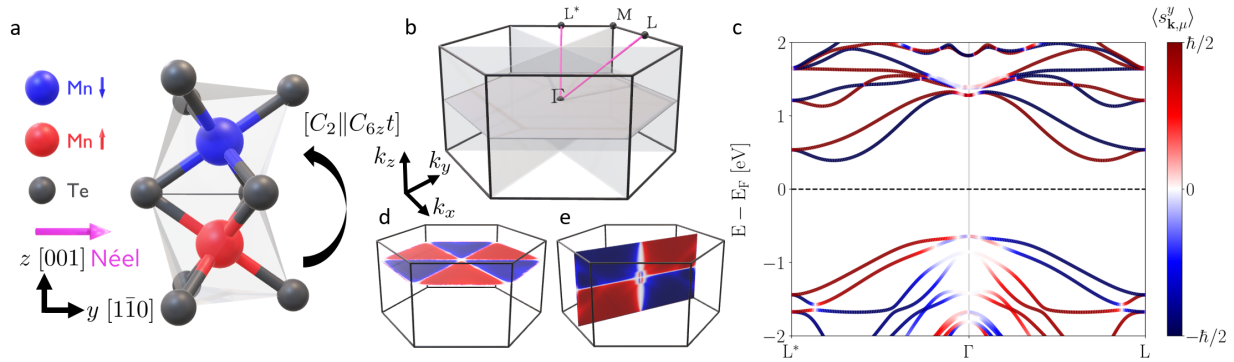


FIG. 1. a) Crystal structure of  $\alpha$ -MnTe together with the octahedral environment that breaks the pure translational and inversion symmetry between the magnetic sublattices. b) Corresponding Brillouin zone in reciprocal space with high symmetry points and highlighted spin degenerate nodal plane structure (gray shaded planes). c) 1D band structure along the pink high symmetry path visualized in b) where red / blue indicates spin-up / spin-down states respectively, white indicates the spin-mixed regions due to SOC. d) and e) show the calculated DFT spin structure of highest valence band for two different planes in the Brillouin zone.

by the polarization of the linearly polarized laser pulse [19]. The spin patterns (cf. Fig. 1 d & e) suggest that such an effect may be arise also for bulk g-wave altermagnets such as  $\alpha$ -MnTe, and we will study the dependence on polarization and incident angle for a specific laser wavelength in the next section.

### III. ANGLE DEPENDENCE OF THE OPTICAL EXCITATION

*Bulk* altermagnets exhibit a more complex nodal-plane structure than *planar* altermagnets, so that it is crucial to investigate the optical excitation in the entire 3D BZ, as opposed to planar altermagnets. Here the qualitative dependence on the laser excitation can be already explained in some detail by considering only a 2D cross section of the BZ [20]. We use the *ab initio* electronic dispersion  $\epsilon_{\mathbf{k}}^{\mu}$  as well as the dipole transition matrix elements  $\mathbf{d}_{\mathbf{k}}^{\mu\nu}$  to characterize the optical excitation by computing the change in the electronic occupation numbers  $n_{\mathbf{k}}^{\mu}$  according to

$$\partial_t n_{\mathbf{k}}^{\mu} = \frac{2\pi}{\hbar} \sum_{\nu} |\mathbf{E}(t) \cdot \mathbf{d}_{\mathbf{k}}^{\mu\nu}|^2 g(\epsilon_{\mathbf{k}}^{\mu} - \epsilon_{\mathbf{k}}^{\nu} \pm \hbar\omega_L) (n_{\mathbf{k}}^{\nu} - n_{\mathbf{k}}^{\mu}) \quad (1)$$

for dipole transitions  $|\mathbf{k}, \mu\rangle \rightarrow |\mathbf{k}, \nu\rangle$  [31, 32]. The time dependent laser pulse is described by  $\mathbf{E}(t)$  and  $g(\Delta\epsilon)$  accounts for the energetic broadened pulse with a Gaussian profile. We describe the angle dependence of the incident laser pulse with  $\hat{\mathbf{e}}_r = (\sin\theta \cos\varphi, \sin\theta \sin\varphi, \cos\theta)^T$  in spherical coordinates.

Figure 2a shows the polarization vector  $\hat{\mathbf{e}}_\alpha$  of the linearly polarized pulse in a plane perpendicular to the propagation direction. The angle  $\alpha$  determines the direction of the polarization as measured against  $\hat{\mathbf{e}}_\theta$ . This relationship can be described by a rotation matrix, which yields the corresponding polarization vector  $\hat{\mathbf{e}}_\alpha$  via

$$\hat{\mathbf{e}}_\alpha := R_{\hat{\mathbf{e}}_r}(\alpha)\hat{\mathbf{e}}_\theta = \{(1 - \cos\alpha)\hat{\mathbf{e}}_r \otimes \hat{\mathbf{e}}_r + \mathbb{1}_{3\times 3} \cos\alpha + [\hat{\mathbf{e}}_r]_\times \sin\alpha\} \hat{\mathbf{e}}_\theta, \quad (2)$$

where  $\otimes$  describes the dyadic product,  $[\hat{\mathbf{e}}_r]_\times$  is the cross product matrix and  $\mathbb{1}_{3\times 3}$  the identity. In the following, we will refer to Fig. 2a for all angles and different vectors.

To characterize the influence of the optical excitation on the spin degree of freedom, we define the *total* spin polarization ( $S_{\text{tot}}^y$ ) and the *excited* spin polarization ( $S_{\text{exc}}^y$ ) in  $y$ -direction as

$$S_{\text{tot}}^y(\hat{\mathbf{e}}_\alpha) = \frac{2\mu_B}{\hbar} \frac{1}{N_k} \sum_{\mathbf{k}, \mu} n_{\mathbf{k}}^\mu(\hat{\mathbf{e}}_\alpha) \langle s_{\mathbf{k}, \mu}^y \rangle \quad \text{and} \quad S_{\text{exc}}^y(\hat{\mathbf{e}}_\alpha) = \frac{2\mu_B}{\hbar} \frac{1}{N_k} \sum_{\substack{\mathbf{k}, \mu \\ \epsilon_{\mathbf{k}}^\mu > E_F}} n_{\mathbf{k}}^\mu(\hat{\mathbf{e}}_\alpha) \langle s_{\mathbf{k}, \mu}^y \rangle, \quad (3)$$

respectively, where  $n_{\mathbf{k}}^\mu(\hat{\mathbf{e}}_\alpha)$  are the occupation numbers that depend on the polarization vector  $\hat{\mathbf{e}}_\alpha$  and  $\langle s_{\mathbf{k}, \mu}^y \rangle$  the spin expectation values, as defined in Sec. II. Note that the excited spin polarization is an essentially non-equilibrium quantity as it arises only from excited carriers above the Fermi energy. The total spin polarization can only be changed via the presence of SOC-induced spin mixing in the electronic states connected by an optical transition.

To investigate the distinctive properties of the *bulk* altermagnet we focus on two distinct directions in the Brillouin Zone. First we will discuss a setup with the laser pulse being oriented along the [001]-direction of the crystal, where the plane perpendicular to that direction shows a spin texture in reciprocal space that is divided by the nodal planes into six triangular areas (cf. Fig. 1d). We study an above-gap excitation with a photon energy of  $3.75 \text{ eV} > 1.44 \text{ eV} = E_{\text{gap}}$  and an excitation angle of  $\alpha = 0^\circ$  (purple polarization vector). Fig. 2b shows the computed electronic distribution in this plane in the first conduction band. The color code for the occupation ranges from zero excited carriers in white to an occupation of 0.5 or more indicated by red, the nodal planes are highlighted by the black lines. The

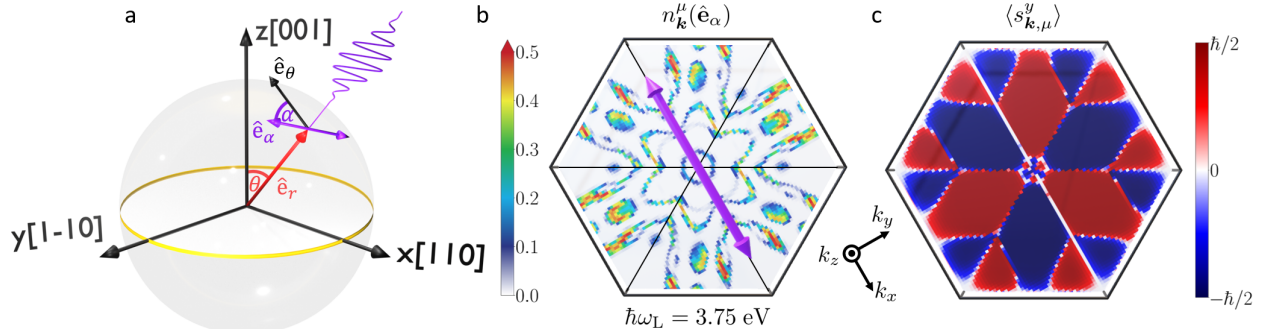


FIG. 2. a) Polarization vector  $\hat{\mathbf{e}}_\alpha$  and the corresponding angles in spherical coordinates. b) 2D cross section of the excited electronic distribution in the first conduction band for a laser pulse oriented along the [001]-direction of the crystal, i.e.  $\theta = 0^\circ$ , with photon energy  $\hbar\omega_L = 3.75$  eV for an excitation angle of  $\alpha = 0^\circ$ . c) Corresponding spin structure of the band.

electronic distribution shows a highly anisotropic excitation pattern. Note that opposite areas exhibit identical electron distribution functions, i.e.,  $n(k_x, k_y, k_z) = n(-k_x, -k_y, k_z)$ .

Combined with the spin texture of the corresponding band, shown in Fig. 2c, this results in a vanishing *excited* spin polarization. Figure 3a i) shows that the same behavior occurs for all excitation angles  $\alpha$  for this particular incident direction of  $\theta = 0^\circ$ . Therefore, it is not possible to excite a spin polarization with a laser pulse in [001]-direction, which already highlights a significant difference of  $\alpha$ -MnTe compared to the planar d-wave altermagnets RuO<sub>2</sub> and KRu<sub>4</sub>O<sub>8</sub> [19].

Next we turn to the case of an incident direction along the [110]-axis of the crystal ( $x$ -direction). For the same photon energy as before we vary the excitation angle  $\alpha$  between  $0^\circ$  and  $180^\circ$ . In this case, we predominantly excite electrons perpendicular to the polarization vector of the laser pulse, which results again in an anisotropic excitation in the band. As Fig. 3c shows for  $\theta = 90^\circ$  the spin structure in the plane now allows for the build up of an excited spin polarization signal. The signal shows a clear sinusoidal dependence changing with one zero as one would expect from planar d-wave altermagnets. We obtain vanishing signals at angles  $0^\circ$  and  $90^\circ$ , and a maximum amplitude around  $60^\circ$  and  $120^\circ$ . Note that the results shown account for all other contributions of excited electrons since the signal is calculated in the entire 3D Brillouin zone. Despite the contributions from the whole BZ, the frequency of the resulting sinusoidal shape can qualitatively be well described by just the 2D cut of the BZ, shown Fig. 3a iii).

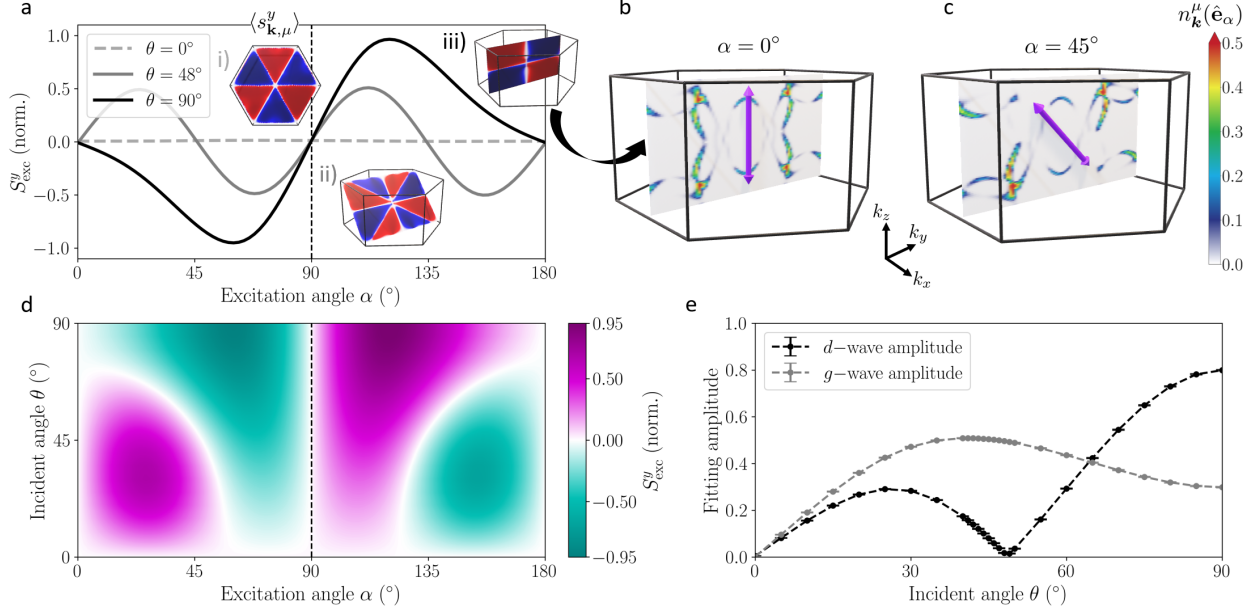


FIG. 3. a) Excited spin polarization as a function of the excitation angle  $\alpha$  for three different incident directions, the insets i)-iii) show the spin structure of a band for a BZ cross-section perpendicular to the laser's incident direction. b) & c) excited carrier distribution in the first conduction band for an incidence angle of  $\theta = 90^\circ$  in the corresponding perpendicular  $k$ -slice. Highlighted are two different polarization directions with b)  $\alpha = 0^\circ$  (no spin polarization) and c)  $\alpha = 45^\circ$  (negative spin polarization). d) Excited spin polarization for all combinations of incident angle  $\theta$  and excitation angle  $\alpha$ . e) Amplitudes of the sinusoidal fit function with d- and g-wave character for different incident directions.

The simple 2D picture introduced above for the spin response also works for other directions of incidence, as we show now. An additional feature appears for intermediate angles, e.g.  $\theta = 48^\circ$  (cf. inset ii)). When we cut through the BZ at this angle and visualize the spin structure of one of the bands in this plane we achieve eight alternating spin sectors, that resemble the spin structure of a planar g-wave altermagnet. This yields a pronounced  $\sin(4\alpha)$ -dependence of  $S_{\text{exc}}^y$  with maxima and minima around odd multiples of  $22.5^\circ$ . The full variation of incident angles  $\theta$  and excitation angles  $\alpha$  can be seen in Fig. 3d, where the excited spin polarization for the given combinations  $(\alpha, \theta)$  is illustrated as a colormap.

We start with a white, i.e. non-spin polarized, region for  $\theta = 0^\circ$  which represents a vanishing signal for [001] incidence. With increasing incidence angle, a spin polarization signal starts to appear, which is at first a combination of  $\sin(2\alpha)$  and  $\sin(4\alpha)$  contributions

as we electrons in both the “planar g-wave” as well as the “planar d-wave” cross section are excited. For  $\theta = 48^\circ$  the signal transitions to a  $\sin(4\alpha)$  dominated behavior because the electrons are now excited predominantly in the “planar g-wave” regions. If we increase the incidence angle further we smoothly traverse from the  $\sin(4\alpha)$  dominated region into the expected “planar d-wave” like  $\sin(2\alpha)$  dominated signal at  $\theta = 90^\circ$ .

The contributions from the “planar d-wave” and “planar g-wave” regions can be disentangled by introducing a fit function

$$f_\theta(\alpha) = A_d^\theta \sin(2\alpha - \phi_d^\theta) + A_g^\theta \sin(4\alpha - \phi_g^\theta) \quad (4)$$

to the excited spin polarization. In Eq. (4),  $A_{d,g}^\theta$  describe the amplitudes of the  $\sin(2\alpha)$  d-wave as well as the  $\sin(4\alpha)$  g-wave contribution, and  $\phi_{d,g}^\theta$  account for an additional phase for each incident direction. The fits are shown in detail in the Supplement S3 of this paper. In Fig. 3e we show the resulting fitting amplitudes  $A_{d,g}^\theta$  as a function of the incidence angle. For normal incidence both of the fitting amplitudes are zero because the signal vanishes. As soon as the incidence angle is increased, a signal with d-wave and g-wave contributions starts to appear, where both amplitudes increase. At around  $25^{circ}$  incidence the d-wave amplitude starts to decrease again until it almost completely gone for an incidence of  $48^\circ$ . Increasing the incidence angle further, the d-wave contribution rises again, while the g-wave contribution shrinks. Finally, the d-wave part becomes larger than the g-wave contribution at approximately  $65^\circ$ . Note that the g-wave contribution is always present in the signal and never vanishes except for  $\theta = 0^\circ$ .

#### IV. WAVELENGTH DEPENDENCE

To complete our study of the optically excited spin polarization we now address its dependence on the laser wavelength to show that the angle dependence discussed so far is rather general for a variety of wavelengths in the visible range. We vary the laser wavelength from  $\hbar\omega_L = 1$  eV to 5 eV to capture all the wavelengths in the visible spectrum. We wish to draw particular attention to the cases with slightly off-normal incidence ( $\theta = 5^\circ$ ), an intermediate angle of incidence with  $\theta = 45^\circ$ , where we expect a dominant “planar g-wave” like dependence and the case with  $\theta = 90^\circ$ , where we expect a dominant “planar d-wave” behavior. We account for a change in absorption of the laser pulse due to the wavelength

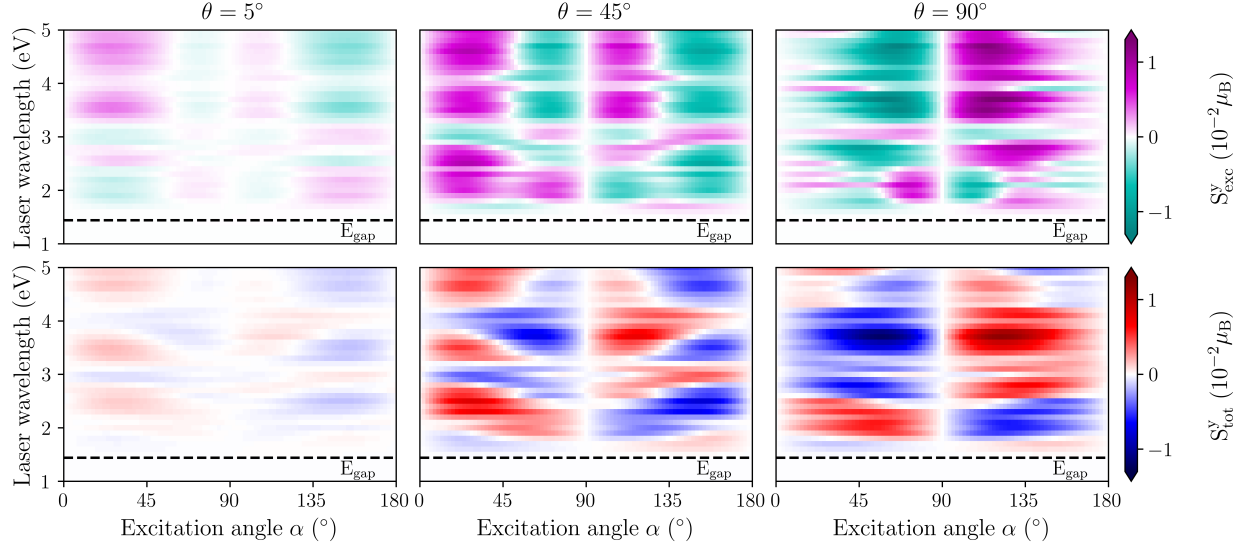


FIG. 4. (a) Excited spin polarization  $S_{\text{exc}}^y$  and (b) total spin polarization  $S_{\text{tot}}^y$  in dependence of the laser wavelength and the excitation angle for different incident laser directions ranging from an incidence angle of  $\theta = 5^\circ$  in the left column over  $\theta = 45^\circ$  in the middle to  $\theta = 90^\circ$  in the right column.

dependent refractive index as described in the Methods section VIB. The results of the wavelength variation can be contained in Fig. 4. The upper row denotes the excited spin polarization  $S_{\text{exc}}^y$  with a color scheme ranging from a negative spin polarization (turquoise) to a positive one (purple). The lower row shows the total spin polarization  $S_{\text{tot}}^y$  indicated with the colors ranging from blue (negative spin polarization) to red (positive spin polarization). In addition we highlight the energy of the band gap ( $E_{\text{gap}}$ ) of  $\alpha$ -MnTe by the black dashed line to show that no spin polarization is excited at all for an excitation with an energy below the band gap. We get only a small signal in the excited and total spin polarization for an incidence close to normal incidence, i.e.  $\theta = 5^\circ$ , for all considered photon energies. In the excited spin polarization for  $\theta = 45^\circ$  and  $\theta = 90^\circ$  we can see the expected  $\sin(4\alpha)$  and  $\sin(2\alpha)$  behavior, respectively, for a large variety of photon energies. In general, the treatment of accounting the signal to be only proportional to the spin structure is too simple since also the orbital character plays an important role for the allowed optical transitions. Furthermore, the number of excited bands influences the signal. This can be seen in the photon energy range from  $E_{\text{gap}}$  up to 2.4 eV, where the computed signal deviates from the expected behavior. This can be accounted to the fact that we only excite contributions

from the first two conduction bands that show an opposite spin character. Thus, the spin polarization is very sensitive to the individual contributions from each of the bands. For higher photon energies, many bands are excited and the spin polarization signal is more likely to follow the general spin structure of the bulk g-wave altermagnet (see supplement S2). An additional altermagnetic feature can be observed in the region around 3 eV. Here, a sign change occurs in the signal since we now dominantly excite bands with the opposite spin character. A similar behavior can be observed for the total spin polarization, thus illustrating that it is also possible to magnetize the sample with optical pulses in the presence of SOC. For comparison, we present a study without the SOC contributions in the supplementary material S1.

## V. CONCLUSION

We showed that it is possible to optically excite an electronic spin-polarization in the prototypical bulk g-wave altermagnet  $\alpha$ -MnTe. The specific altermagnetic spin structure together with the anisotropic electron distributions in  $k$ -space driven by linearly polarized optical pulses make a coherent control of spins in magnetically compensated materials possible. In difference to d-wave systems, the angle of incidence of the excitation pulse has an important influence in bulk g-wave altermagnets. Depending on this angle, the induced spin polarization shows different periodicities with respect to the excitation angle of the exciting linearly polarized pulse. In particular, for special angles of incidence the periodicity of the induced spin polarization resembles that of a planar d-wave system, but the six-fold symmetry of the crystal structure is never reflected in the excited spin polarization. Our study is intended to motivate and guide further magneto-optical experiments on altermagnetic candidate materials. We presented a simple and straightforward way to predict the periodicity of the spin signal from the spin structure in a plane perpendicular to the incidence direction of the laser pulse. In addition, we showed that experiments that measure this non-equilibrium electronic spin polarization can serve as a probe of the bulk altermagnetic character.

## ACKNOWLEDGMENTS

Funded by the Deutsche Forschungsgemeinschaft (DFG, German Research Foundation) – TRR 173 – 268565370 (projects A03 and A08).

## VI. METHODS

### A. DFT+U calculations

In order to account for the strongly correlated electrons of Mn, the Hubbard parameters for the Mn  $3d$ -orbitals were set to  $U = 4.0$  eV and  $J = 0.97$  eV [10] within the fully localized limit (FLL) scheme of the ELK Code [26, 28]. To ensure tight convergence, the calculations are carried out on a  $26 \times 26 \times 16$   $k$ -grid. The structure shows an antiferromagnetic ordering at the two inequivalent Mn sites, converging with a magnetic moment of  $4.447 \mu_B$  per Mn atom in the unit cell. Moreover, a slight canting of the Manganese magnetic moments can be observed due to spin-orbit coupling (SOC) resulting in a very small ferromagnetic moment of  $3.7 \cdot 10^{-4} \mu_B$  in the  $[001]$ -direction. This finding aligns with those reported in previous studies [10, 12, 33].

### B. Dielectric Function

To characterize the wavelength dependence of the absorption and reflection in  $\alpha$ -MnTe, we calculated the dielectric tensor  $\underline{\epsilon}(q \rightarrow 0, \omega)$  within the random phase approximation (RPA) in the wavelength range from  $\hbar\omega_L = 0$  eV to  $\hbar\omega_L = 5$  eV. We increased the number of  $k$ -points to  $32 \times 32 \times 20$  and adjusted the smearing width to 0.003 Ha to eliminate artificial artefacts that result from the  $k$ -point mesh. The results are shown in Fig. 5. They qualitatively match the results shown in Refs. [21, 34], showing a peak in the real part of the dielectric function around 2 eV. The birefringent character of hexagonal  $\alpha$ -MnTe is apparent as two of the diagonal components are equal ( $\epsilon_{xx} = \epsilon_{yy} \neq \epsilon_{zz}$ ). From the dielectric function we calculate the complex refractive index  $\tilde{n}(\omega) = n(\omega) + i\kappa(\omega)$ , where  $n(\omega)$  is the real refractive index and  $\kappa(\omega)$  the extinction coefficient. To consider the reduction of the electric field amplitude we assume an effective refractive index that results from the mean value of the three Cartesian directions  $\bar{n} = (n_{xx} + n_{yy} + n_{zz})/3$ . Based on this assumption,

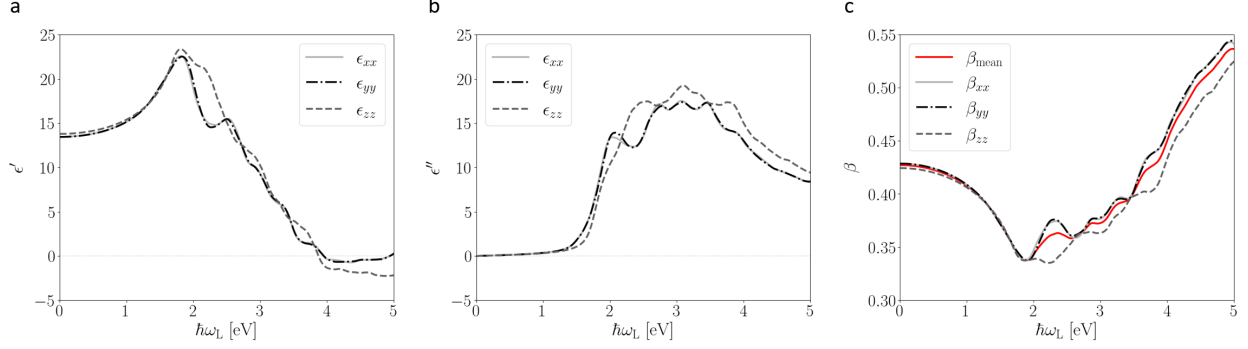


FIG. 5. a) real part and b) imaginary part of the dielectric function for bulk  $\alpha$ -MnTe. c) corresponding reduction factor for the electric field amplitude.

the factor

$$\beta_{\text{mean}}(\omega) = \frac{2}{\sqrt{[1 + \bar{n}(\omega)]^2 + \bar{\kappa}(\omega)^2}} \quad (5)$$

determines the reduction of the electric field amplitude  $E'_0(\omega) = E_0\beta(\omega)$  in the material at a given wavelength. The laser pulse is modeled by a Gaussian envelope

$$\mathbf{E}(t) = E'_0(\omega_L)\hat{\mathbf{e}}_\alpha \exp\left[-4\ln(2)\frac{t^2}{\tau_{\text{FWHM}}^2}\right] \quad (6)$$

where  $\omega_L$  is the laser frequency,  $\hat{\mathbf{e}}_\alpha$  the polarization vector defined in Sec. III and  $\tau_{\text{FWHM}} = 40$  fs the full width at half maximum. The pump fluence is determined by

$$\rho_E = \frac{1}{2}\epsilon_0 c \int_{-\infty}^{\infty} |\mathbf{E}(t)|^2 dt = \frac{1}{4}E_0^2 \epsilon_0 c \sqrt{\frac{\pi}{2\ln(2)}} \tau_{\text{FWHM}}. \quad (7)$$

Thus we calculate the electric field amplitude for a fixed fluence of  $\rho_E = 4 \frac{\text{mJ}}{\text{cm}^2}$  according to

$$E_0 = \left[ \frac{4\rho_E}{\epsilon_0 \tau_{\text{FWHM}} c} \sqrt{\frac{2\ln(2)}{\pi}} \right]^{1/2}. \quad (8)$$

to have a good comparison with experiments.

---

[1] L. Šmejkal, J. Sinova, and T. Jungwirth, Phys. Rev. X **12**, 031042 (2022).

[2] L. Šmejkal, J. Sinova, and T. Jungwirth, Phys. Rev. X **12**, 040501 (2022).

[3] C. Song, H. Bai, Z. Zhou, L. Han, H. Reichlova, J. H. Dil, J. Liu, X. Chen, and F. Pan, Nature Reviews Materials (2025).

- [4] L. Bai, W. Feng, S. Liu, L. Šmejkal, Y. Mokrousov, and Y. Yao, *Advanced Functional Materials* **34**, 2409327 (2024).
- [5] Z. Guo, X. Wang, W. Wang, G. Zhang, X. Zhou, and Z. Cheng (2025), <https://arxiv.org/abs/2503.22173>.
- [6] O. Fedchenko, J. Minár, A. Akashdeep, S. W. D'Souza, D. Vasilyev, O. Tkach, L. Odenbreit, Q. Nguyen, D. Kutnyakhov, N. Wind, L. Wenthaus, M. Scholz, K. Rosnagel, M. Hoesch, M. Aeschlimann, B. Stadtmüller, M. Kläui, G. Schönhense, T. Jungwirth, A. B. Hellenes, G. Jakob, L. Šmejkal, J. Sinova, and H.-J. Elmers, *Science Advances* **10**, eadj4883 (2024).
- [7] Z. Feng, X. Zhou, L. Šmejkal, L. Wu, Z. Zhu, H. Guo, R. González-Hernández, X. Wang, H. Yan, P. Qin, X. Zhang, H. Wu, H. Chen, Z. Meng, L. Liu, Z. Xia, J. Sinova, T. Jungwirth, and Z. Liu, *Nature Electronics* **5**, 735 (2022).
- [8] P. Keßler, L. Garcia-Gassull, A. Suter, T. Prokscha, Z. Salman, D. Khalyavin, P. Manuel, F. Orlandi, I. I. Mazin, R. Valentí, and S. Moser, *npj Spintronics* **2**, 50 (2024).
- [9] M. Hiraishi, H. Okabe, A. Koda, R. Kadono, T. Muroi, D. Hirai, and Z. Hiroi, *Phys. Rev. Lett.* **132**, 166702 (2024).
- [10] R. D. Gonzalez Betancourt, J. Zubáč, R. Gonzalez-Hernandez, K. Geishendorf, Z. Šobáň, G. Springholz, K. Olejník, L. Šmejkal, J. Sinova, T. Jungwirth, S. T. B. Goennenwein, A. Thomas, H. Reichlová, J. Železný, and D. Kriegner, *Phys. Rev. Lett.* **130**, 036702 (2023).
- [11] R. D. Gonzalez Betancourt, J. Zubáč, K. Geishendorf, P. Ritzinger, B. Růžičková, T. Kotte, J. Železný, K. Olejník, G. Springholz, B. Büchner, A. Thomas, K. Výborný, T. Jungwirth, H. Reichlová, and D. Kriegner, *npj Spintronics* **2**, 45 (2024).
- [12] J. Krempaský, L. Šmejkal, S. W. D'Souza, M. Hajlaoui, G. Springholz, K. Uhlířová, F. Alarab, P. C. Constantinou, V. Strocov, D. Usanov, W. R. Pudelko, R. González-Hernández, A. Birk Hellenes, Z. Jansa, H. Reichlová, Z. Šobáň, R. D. Gonzalez Betancourt, P. Wadley, J. Sinova, D. Kriegner, J. Minár, J. H. Dil, and T. Jungwirth, *Nature* **626**, 517 (2024).
- [13] T. Osumi, S. Souma, T. Aoyama, K. Yamauchi, A. Honma, K. Nakayama, T. Takahashi, K. Ohgushi, and T. Sato, *Phys. Rev. B* **109**, 115102 (2024).
- [14] S. Lee, S. Lee, S. Jung, J. Jung, D. Kim, Y. Lee, B. Seok, J. Kim, B. G. Park, L. Šmejkal, C.-J. Kang, and C. Kim, *Phys. Rev. Lett.* **132**, 036702 (2024).
- [15] A. Hariki, A. Dal Din, O. J. Amin, T. Yamaguchi, A. Badura, D. Kriegner, K. W. Edmonds, R. P. Campion, P. Wadley, D. Backes, L. S. I. Veiga, S. S. Dhesi, G. Springholz, L. Šmejkal,

- K. Výborný, T. Jungwirth, and J. Kuneš, Phys. Rev. Lett. **132**, 176701 (2024).
- [16] D. Y. Kazmin, V. Esin, Y. S. Barash, A. Timonina, N. Kolesnikov, and E. Deviatov, Physica B: Condensed Matter **696**, 416602 (2025).
- [17] K. P. Kluczyk, K. Gas, M. J. Grzybowski, P. Skupiński, M. A. Borysiewicz, T. Faş, J. Sufczyński, J. Z. Domagala, K. Graszka, A. Mycielski, M. Baj, K. H. Ahn, K. Výborný, M. Sawicki, and M. Gryglas-Borysiewicz, Phys. Rev. B **110**, 155201 (2024).
- [18] O. J. Amin, A. Dal Din, E. Golias, Y. Niu, A. Zakharov, S. C. Fromage, C. J. B. Fields, S. L. Heywood, R. B. Cousins, F. Maccherozzi, J. Krempaský, J. H. Dil, D. Kriegner, B. Kiraly, R. P. Champion, A. W. Rushforth, K. W. Edmonds, S. S. Dhesi, L. Šmejkal, T. Jungwirth, and P. Wadley, Nature **636**, 348 (2024).
- [19] M. Weber, S. Wust, L. Haag, A. Akashdeep, K. Leckron, C. Schmitt, R. Ramos, T. Kikkawa, E. Saitoh, M. Kläui, *et al.*, arXiv preprint arXiv:2408.05187 (2024).
- [20] M. Weber, K. Leckron, L. Haag, R. Jaeschke-Ubiergo, L. Šmejkal, J. Sinova, and H. C. Schneider, arXiv preprint arXiv:2411.08160 (2024).
- [21] I. I. Mazin, Phys. Rev. B **107**, L100418 (2023).
- [22] M. Vila, V. Sunko, and J. E. Moore, arXiv preprint arXiv:2410.23513 (2024).
- [23] Z. Zhou, S. Sharma, J. K. Dewhurst, and J. He, arXiv preprint arXiv:2502.01258 (2025).
- [24] A. Eskandari-asl, J. I. Facio, O. Janson, A. Avella, and J. v. d. Brink, arXiv preprint arXiv:2504.01640 (2025).
- [25] I. Gray, Q. Deng, Q. Tian, M. Chilcote, J. S. Dodge, M. Brahlek, and L. Wu, Applied Physics Letters **125**, 212404 (2024).
- [26] J. K. Dewhurst et al., The Elk Code, <http://elk.sourceforge.net/>.
- [27] J. P. Perdew, K. Burke, and M. Ernzerhof, Phys. Rev. Lett. **77**, 3865 (1996).
- [28] A. I. Liechtenstein, V. I. Anisimov, and J. Zaanen, Phys. Rev. B **52**, R5467 (1995).
- [29] D. Kriegner, H. Reichlova, J. Grenzer, W. Schmidt, E. Ressouche, J. Godinho, T. Wagner, S. Y. Martin, A. B. Shick, V. V. Volobuev, G. Springholz, V. Holý, J. Wunderlich, T. Jungwirth, and K. Výborný, Phys. Rev. B **96**, 214418 (2017).
- [30] D. Litvin and W. Opechowski, Physica **76**, 538 (1974).
- [31] S. Essert and H. C. Schneider, Phys. Rev. B **84**, 224405 (2011).
- [32] M. Stiehl, M. Weber, C. Seibel, J. Hofer, S. T. Weber, D. M. Nenno, H. C. Schneider, B. Rethfeld, B. Stadtmüller, and M. Aeschlimann, Applied Physics Letters **120** (2022).

[33] I. I. Mazin and K. D. Belashchenko, Phys. Rev. B **110**, 214436 (2024).

[34] J. Oleszkiewicz, A. Kisiel, and S. Ignatowicz, Thin Solid Films **157**, 1 (1988).

**Supplement to**  
**Optical signatures of bulk g-wave antiferromagnetism in MnTe**

Luca Haag,<sup>1</sup> Marius Weber,<sup>2,1</sup> Kai Leckron,<sup>1</sup> Libor  
Šmejkal,<sup>3,4</sup> Jairo Sinova,<sup>2</sup> and Hans Christian Schneider<sup>1</sup>

<sup>1</sup>*Department of Physics and Research Center OPTIMAS,*

*University of Kaiserslautern-Landau, 67663 Kaiserslautern, Germany*

<sup>2</sup>*Institut für Physik, Johannes Gutenberg University Mainz, 55099 Mainz, Germany*

<sup>3</sup>*Max Planck Institute for the Physics of Complex Systems, 01187 Dresden, Germany*

<sup>4</sup>*Max Planck Institute for Chemical Physics of Solids, 01187 Dresden, Germany*

(Dated: May 19, 2025)

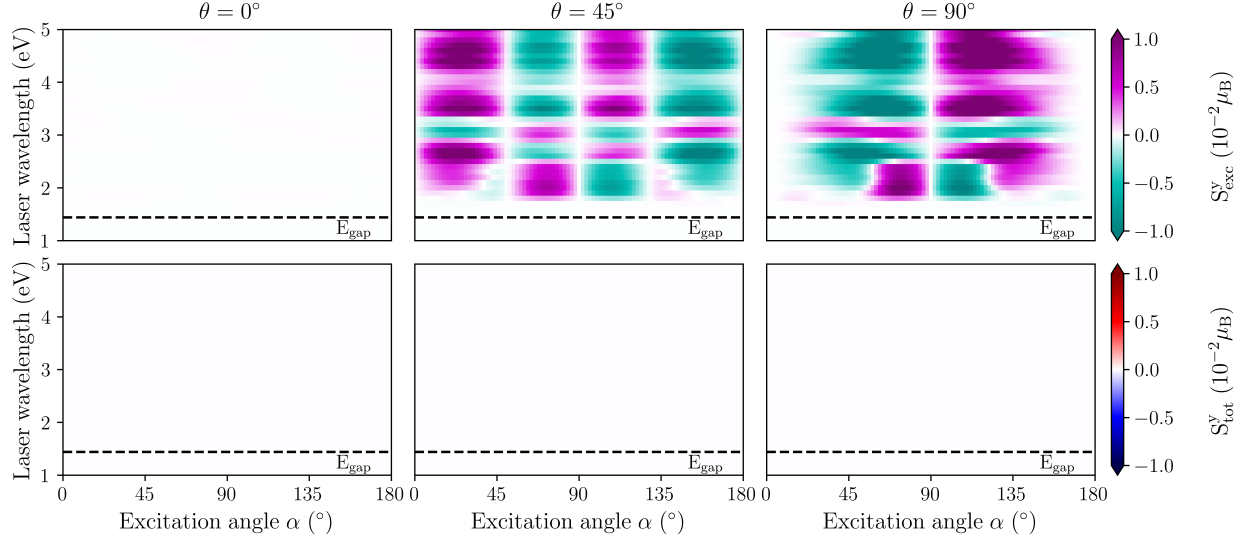


FIG. S1. Laser wavelength dependence when neglecting spin-orbit coupling. a)-c) shows the excited spin polarization and d)-f) the total spin polarization for different incident angles.

## S1. EXCITATION WITHOUT SOC

In this section we demonstrate that the contributions of the spin polarization induced in the excited states and their symmetries does not arise due to the influence of spin-orbit coupling (SOC). Figure S1 d)-f) shows the the wavelength dependence of the excited and total spin polarization without SOC in the underlying ab-initio calculation, which should be compared with Fig. 4 in the main manuscript. In difference to Fig. 4 in the main text, excitations are now only possible by a spin conserving transition which is reflected in the vanishing total spin polarization. In Fig. S1 a), for normal incidence, also the excited spin polarization vanishes for every wavelength and polarization angle, as expected by the symmetries discussed in the main text. In Fig S1 b) we changed the incidence angle to  $45^\circ$ , and then obtain a signal with the expected  $\sin(4\alpha)$ -like behavior for most of the photon energies. Compared to the case with SOC in the manuscript, the main difference is that the angles for which the spin polarization vanishes do not change for all laser wavelengths. The signal deviates from the expected behavior in the energy range from  $E_{\text{gap}}$  to about 2.5 eV as discussed in the main text of the paper.

We now focus on the position of the zeros in the spin polarization signal. Referring to the schematic spin arrangement in the bulk g-wave altermagnet in Fig. S2 a), we can

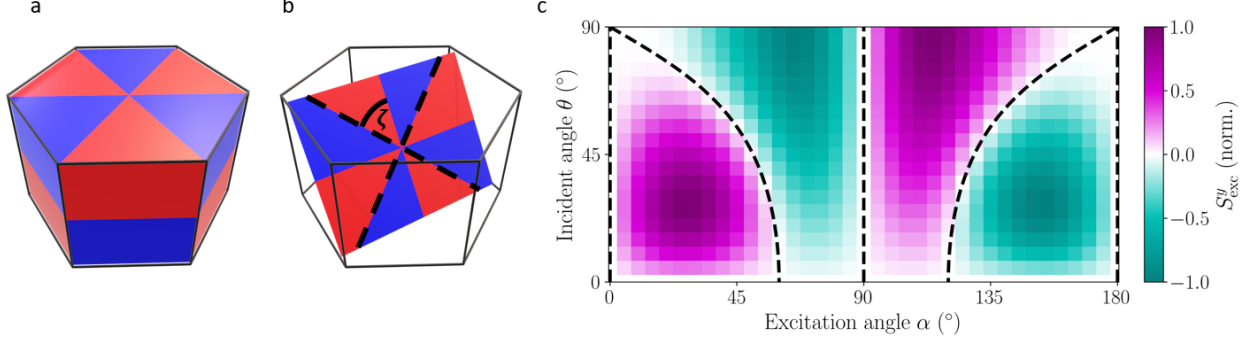


FIG. S2. a) Schematic spin arrangement of the bulk g-wave altermagnet in the entire 3D BZ, b) spin texture of the 2D cut through the BZ, with the nodal plane angle  $\zeta$  is highlighted. c) computed excited spin polarization for a photon energy of  $\hbar\omega_L = 3.50$  eV for different incidence and excitation angles. Dashed black lines represent the excitation angles at which a nodal plane is observed in the 2D cut of the BZ, perfectly matching the roots in the spin polarization signal.

track the position of the nodal planes with respect to the incidence angle  $\theta$ . Independent of the incidence angle, Fig. S2 b) shows that we always have a nodal plane at the excitation angles  $\alpha = 0^\circ$ ,  $\alpha = 90^\circ$  and  $\alpha = 180^\circ$ . The additional nodal plane in the 2D cut of the BZ, shown as black dashed line in Fig. S2 b), changes its position depending on  $\theta$ . In the case without SOC the excitation angle  $\zeta$  at which this nodal plane occurs can be analytically defined by the expression

$$\zeta(\theta) = \arccos\left(\frac{1}{\sqrt{1 + 3\cos^2(\theta)}}\right). \quad (\text{S1})$$

In Fig. S2 c) we calculated the dependence of the excited spin polarization on the incident angle for a fixed photon energy of  $\hbar\omega_L = 3.50$  eV without SOC contributions. The color code used here is the same as for the excited spin polarization in the main manuscript. The black dashed lines show the expected nodal plane positions. One can see a perfect match between these and the roots in the spin polarization signal. Thus highlighting, the remarkable agreement between the spin polarization signal and the bulk g-wave spin order.

## S2. EXCITATION ALONG A 1D-PATH

In the main text and in the previous section we demonstrated that the signal in the excited spin polarization differs from the expected behavior for photon energies in the range

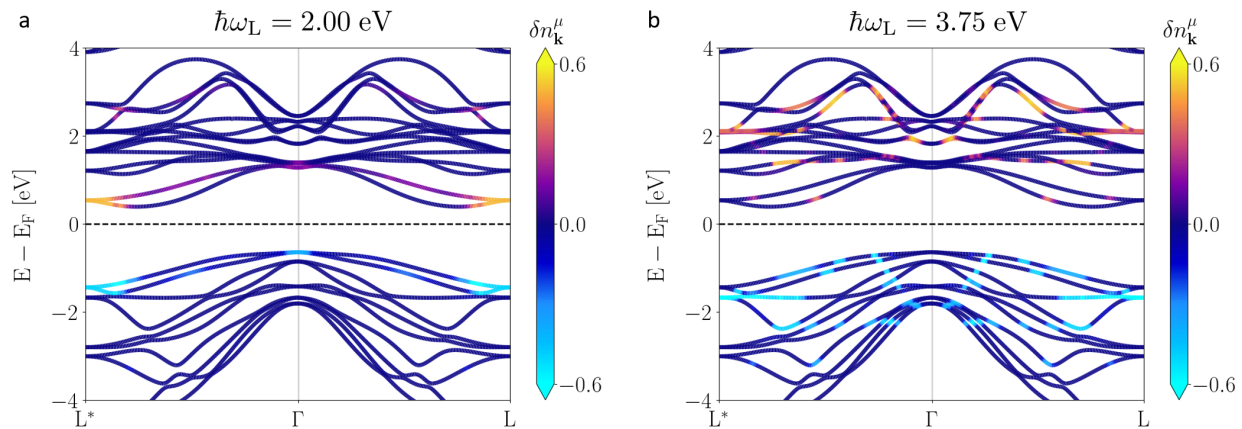


FIG. S3. Change in the electronic occupation when exciting  $\alpha$ -MnTe with a laser pulse with normal incidence and  $\alpha = 0^\circ$ . Shown is the change along the 1D-path  $L^* - \Gamma - L$  for a photon energy of a)  $\hbar\omega_L = 2.00$  eV and b)  $\hbar\omega_L = 3.75$  eV to illustrate the number of excited bands. Here SOC is included.

of 1.44 eV to roughly 2.5 eV. To check why these deviations appear we now take a look at the optical transitions that occur for two different photon energies along the 1D-path  $L^* - \Gamma - L$ . Figure S3 shows the change in the electronic occupation  $\delta n_{\mathbf{k}}^\mu$  with the loss of electronic distribution in the valence bands indicated by cyan and the increase of electronic distribution in the conduction band indicated by yellow. For a photon energy of  $\hbar\omega_L = 2.00$  eV, one can see in Fig. S3a) that the main contributions involve only transitions into the first two conduction bands. When computing the excited spin polarization signal, it is largely affected by the individual contributions from these two bands. The optical transition matrix elements take into account the spin and orbital character of the electronic Bloch wave functions computed from DFT. Therefore, the dependence on the polarization vector of the electric field in general is complex. In this case the spin polarization signal does not show a direct correspondence to the spin structure of the bulk  $g$ -wave altermagnet. If we excite with a larger photon energy, e.g.  $\hbar\omega_L = 3.75$  eV many conduction bands are excited. Figure S3 b) shows that, in this instance, we get significant contributions from numerous individual bands to the excited spin polarization, leading to a signal that shows a good correspondence to the underlying bulk  $g$ -wave spin structure.

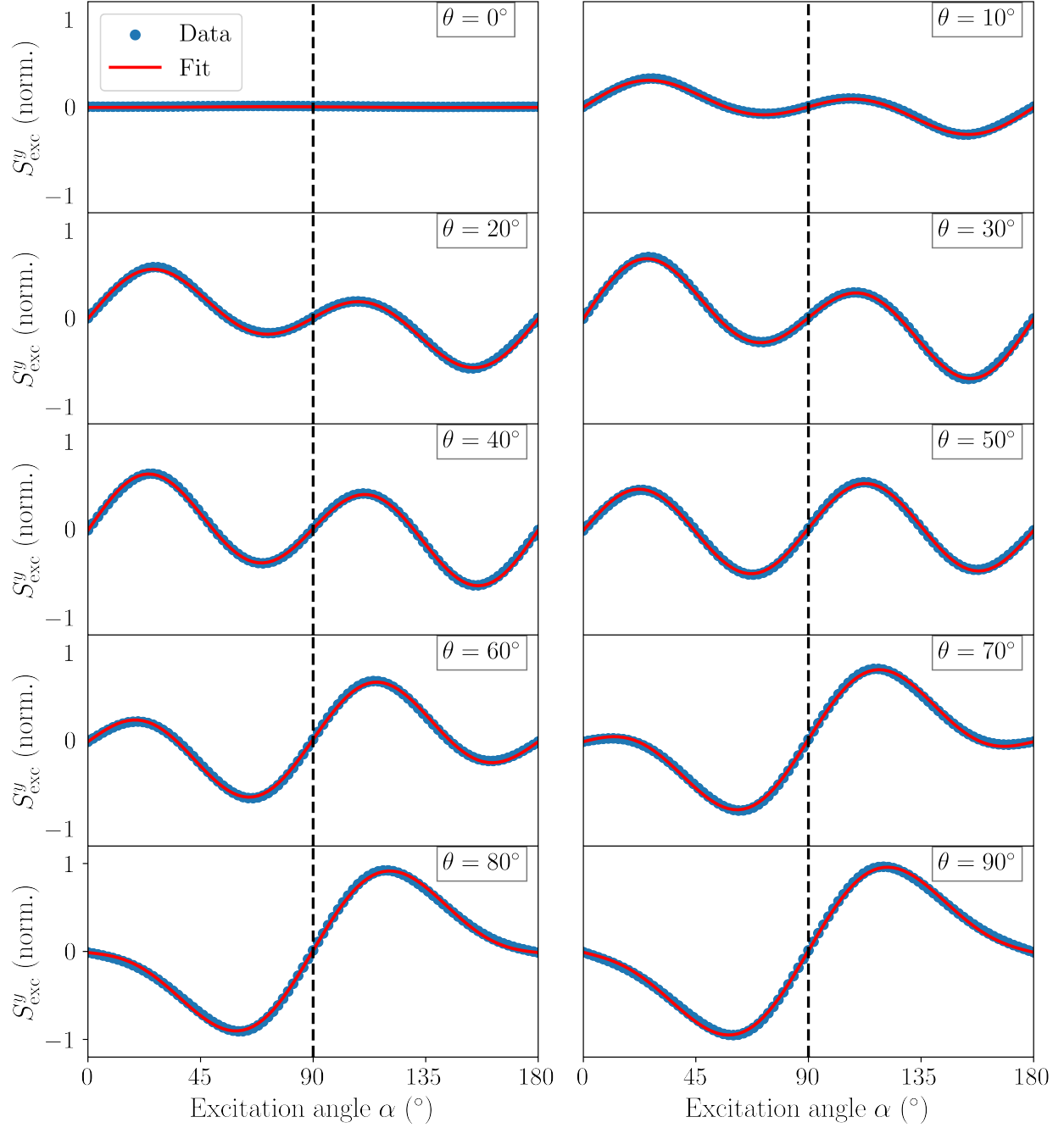


FIG. S4. Excited spin polarization for different incident angles  $\theta$ . The data computed for a photon energy of  $\hbar\omega_L = 3.75$  eV is shown as blue dots. The sinusoidal fit functions  $f_\theta(\alpha)$  are shown in red.

### S3. SINUSOIDAL FITS

In this section we discuss the sinusoidal fit functions

$$f_{\theta}(\alpha) = A_{\text{d}}^{\theta} \sin(2\alpha - \phi_{\text{d}}^{\theta}) + A_{\text{g}}^{\theta} \sin(4\alpha - \phi_{\text{g}}^{\theta})$$

that have been applied to the data computed in the main manuscript in more detail. Figure S4 illustrates the excited spin polarization for a photon energy of  $\hbar\omega_{\text{L}} = 3.75$  eV calculated using our optical model (blue dots), for various incident angles of the laser pulse. On top of these, the sinusoidal fits are shown as red solid lines. Overall, the fit functions are in very good agreement with the computed data. This indicates that the main features of the spin polarization induced in bulk g-wave altermagnets can be captured by this simple model that takes into account “planar d-wave” and “planar g-wave” signatures.